Structure and Rheology of Aramid Solutions: X-ray Scattering Measurements

Stephen J. Picken,* Jozef Aerts, Rob Visser, and Maurits G. Northolt

Akzo Research Laboratories Arnhem, Corporate Research, Physical Chemistry Department, P.O. Box 9300, 6800 SB Arnhem, The Netherlands

Received November 13, 1989; Revised Manuscript Received February 16, 1990

ABSTRACT: Preliminary results are presented on the orientational order in the lyotropic nematic phase of poly(4,4′-benzanilidyleneterephthalamide) in concentrated H_2SO_4, using synchrotron X-ray scattering, both during and after simple shear deformation. The average orientational order, as measured from the azimuthal peak width of the 003 reflection, is almost independent of the shear rate. This is contrary to the results obtained from microscopic observation, where the degree of orientation appears to increase with increasing shear rate. The development of the orientation, as determined by X-ray scattering, during a start-up experiment depends on the applied strain. This observed strain dependence is compared to an affine simple shear deformation model. The relaxation time of the shear-induced orientation decreases with increasing initial shear rate. During coagulation experiments the meridional reflections move to slightly smaller Bragg angles, indicating that chain stretching occurs.

Introduction

To study the complex rheological behavior of polymer liquid crystals, we have performed measurements of the orientational order in aramid solutions both during and after simple shear flow. It has been shown that during start-up experiments the structure of aramid solutions changes dramatically.[1] This was concluded both from transient shear-stress measurements and from light intensity measurements. Here we present some preliminary results from X-ray scattering experiments. The advantage of using X-ray scattering compared to other scattering techniques (e.g., SALS) is the easier interpretation of the results due to the well-known structure of the scattering entities (the polymer chains) and the absence of multiple scattering. With optical methods the results are strongly influenced by the presence of disclinations in the director field.

We used an aramid solution consisting of poly(4,4′-benzanilidyleneterephthalamide) (DABT) in concentrated H_2SO_4 (99.8% (w/w)). The orientational order was measured by wide-angle X-ray scattering. Due to the low scattering intensity of aramid solutions and the possibility of coagulation due to the presence of water vapor, we used the synchrotron radiation source at the Daresbury laboratory (beamline 7.2). This allows very short exposure times for the X-ray films (ca. 30 s). Also, with these short exposure times, the development and relaxation of the orientational order can be studied during and after a shear experiment.

The plan of this paper is as follows: First we will describe the method to obtain the average orientational order from the X-ray films and will give some results for the transient shear flow and relaxation experiments. Next we will describe the influence of coagulation on the meridional reflections. Finally we will discuss the results and draw some conclusions.

Experimental Section

We studied a solution consisting of 20% (w/w) poly(4,4′-benzanilidyleneterephthalamide) (DABT, Figure 1) dissolved in concentrated H_2SO_4. The sulfuric acid had a concentration of ca. 99.8%. The polymer sample had a molecular weight of ca. 30 000 as determined from the viscosity of a solution at a standardized concentration. The calibration curve that was used was obtained for PPTA (poly(*p*-phenyleneterephthalamide)) in H_2SO_4, using various methods such as GPC and end-group analysis. This means that the molecular weight given for the DABT sample is only an estimate.

DABT

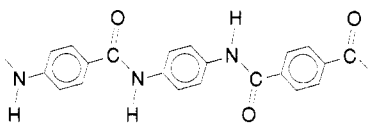

Figure 1. The aramid DABT (poly(4,4′-benzanilidyleneterephthalamide)).

The DABT polymer was used rather than PPTA, which is generally used for aramid fiber spinning, because DABT solutions are liquid crystalline at room temperature. Therefore shear experiments can be performed without the use of an oven around the shear cell.

In Figure 2 we show the steady-state viscosity (i.e., at large strain) of the 20% (w/w) DABT solution at room temperature. The results were obtained with a Rheometrics RMS-605 rheometer (plate–plate geometry, gap 1 mm, radius 12.5 mm). A reasonable agreement with power-law behavior ($\sigma = K\dot{\gamma}^n$) is observed, with parameters K = 1150 Pa s and n = 0.32. This shear thinning behavior is well-known for aramid solutions. However, the value of n is much lower than is observed at elevated temperature for a 19.8% (w/w) PPTA solution of similar molecular weight: K = 166 Pa s, n = 0.7 at 80 °C.

An exploded view of the sample cell is shown in Figure 3. Thin mica foil (20 μm) is glued to the glass slides to allow the X-ray radiation to pass through the sample. The unsupported width of the mica foils is ca. 2 mm. The glass slides are mounted in a special shear flow cell, using tungsten ribbons 50 μm thick as spacers. The upper plate is displaced at a constant velocity to obtain a constant shear rate. Ten different shear rates were used, from 0.25 to 250 s^{-1}. The sample thickness is not accurately known as the mica foil will probably bend slightly, due to the high viscosity of the solution. This means that the actual shear rate will be slightly less than the calculated value (velocity/spacer thickness). However, we did not observe any large differences in the turbidity in the sample between the supported and the unsupported part of the mica foils, so that the sample thickness was quite uniform. This means that the error in the shear rate due to the bending of the unsupported part of the mica foils is not a serious problem. From microscopic observation of a sample similar to the one we used, we estimate that the error in the shear rate is at most ~20%. The shear flow cell and the driving unit were originally designed for polarization microscopy measurements and are described in ref 2. The sample cell was connected to the driving unit with a Bowden cable so that the

0024-9297/90/2223-3849$02.50/0

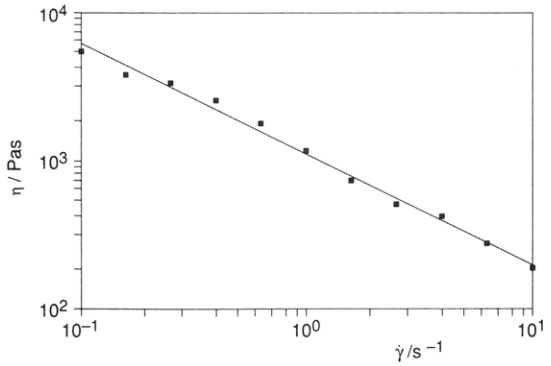

Figure 2. Steady-state viscosity of a 20% (w/w) DABT solution ($\bar{M}_w$ = 30 000, plate–plate geometry, 1-mm gap, 12.5-mm radius, T = 20 °C).

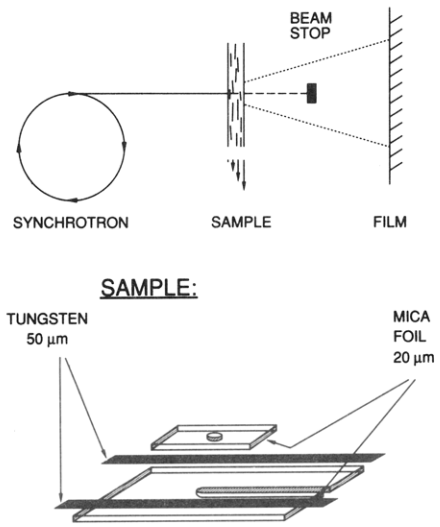

Figure 3. Schematic drawing of the construction of the shear flow cell. To let the X-ray radiation pass through the sample, a slit and a hole have respectively been ground into the top and bottom glass slides. Mica foil of ca. 20 μm is glued onto the glass slides with a low-viscosity epoxy adhesive. The distance between the slides is determined by tungsten ribbons, 50 μm thick. The unsupported width of the mica foils is ca. 2 mm.

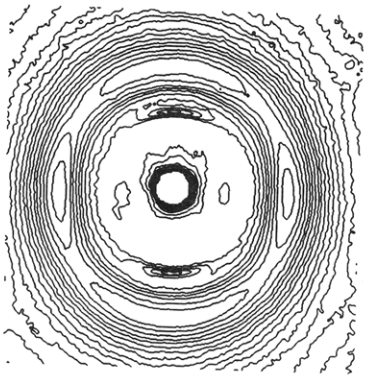

Figure 4. Contour plot of a typical X-ray diffraction pattern, showing the 003 meridional reflection, the weak equatorial reflection, and the slightly oriented H_2SO_4 ring. For the d values, see Table I.

position of the sample with the respect to the X-ray beam could be adjusted easily. The distance from the flow cell to the X-ray film was calibrated by using Si powder. The wavelength of the X-ray radiation was 0.1488 nm.

Results

(i) Observed Reflections. In Figure 4 we show a contour plot of a typical diffraction pattern. The contour plot was obtained with a Teragon-Context GOP302 image analyzer. We observe sharp meridional reflections (only one of these is visible in Figure 4), a diffuse equatorial reflection, and a slightly oriented H_2SO_4 ring.

Table I
Observed Reflections of a 20% (w/w) DABT Solution ($\bar{M}_w$ = 30 000)[a]

d value/nm	hkl index	c axis/nm
0.618 (0.001)	003	1.854 (0.003)
0.466 (0.001)	004	1.864 (0.004)
0.310 (0.001)	006	1.860 (0.006)
0.208 (0.001)	009	1.872 (0.009)
0.86 (0.01)	b	
0.41 (0.01)	c	

[a] The listed d values are average values from different films; standard deviations are given in parentheses. [b] Highly oriented broad equatorial reflection. [c] Sulfuric acid ring with slight orientation.

The reflections that were found for an oriented DABT solution are listed in Table I. The d values are calculated by using the Bragg equation ($d = \lambda/(2 \sin(\theta))$). The order of the reflection is expressed in the form of a Miller index hkl where each index corresponds to a direction of the reciprocal lattice. Here we are dealing with a uniaxial nematic phase so that only the c axis (parallel to the molecular chains) gives rise to sharp meridional reflections. The length of the c axis of the unit cell is calculated by multiplying the order of the reflection by the measured d value. As expected the meridional reflections are slightly asymmetric in the radial direction.[3]

The $00l$ reflections correspond to a monomer length of 1.863 (0.004) nm (average c-axis value); this agrees well with results from a space-filling model of the polymer (1.88 nm). The polymer is made from terephthaloyl dichloride and 4,4′-diaminobenzanilide so that we may expect an irregular orientation of the amide bond in the diamine. This means that we are dealing with an irregular polymer chain (random copolymer).

From the broad equatorial reflection it is evident that in these aramid solutions there is little lateral correlation between individual molecules. This means that we are dealing with more or less isolated individual chains, so that the degree of alignment of the chains can in principle be obtained by scanning over the $00l$ reflections. It is noted that the interpretation of such results is complicated by the fact that the local structure in aramid solutions is not well understood. We expect the meridional reflections to be broadened by layer lines. In the section on the experimental determination of order parameters and the discussion we will deal with this effect in more detail.

We note a systematic increase in the c-axis value with increasing order of the reflections. This trend is explained in the section on the coagulation experiments, using a wormlike model for the polymer chains.

(ii) Determination of an Experimental Orientational Order Parameter. The azimuthal orientation of the 003 reflection was used as a measure for the average orientational order of the solution. The method consists of measuring the full width at half-maximum (fwhm) of this reflection either by using a densitometer (Joyce-Loebl) or by using an image analysis system (Olympus, CUE-2). The fwhm can be measured reasonably well with an image analysis system and has the additional advantage that the time required to analyze a film is much shorter than with the densitometer.

In Figure 5 we show the optical density as a function of the azimuthal angle β for a 003 reflection. The drawn circles correspond to a calculated distribution of the form

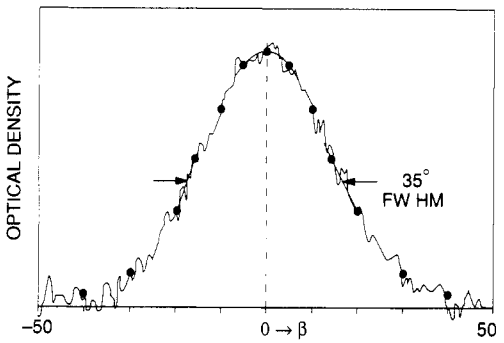

Figure 5. Densitogram of an azimuthal scan over a 003 reflection; the drawn circles correspond to a mean-field-like distribution as given in eq 2.

$$f(\beta) = \frac{1}{Z}\exp[\alpha(P_2(\cos(\beta)))] \quad (1)$$

where Z is a normalization constant, α determines the width of the distribution, and $P_2(\cos(\beta))$ is the second-order Legendre polynomial of $\cos(\beta)$: $P_2(\cos(\beta)) = (3\cos^2(\beta) - 1)/2$.

The Maier–Saupe model for the nematic phase[4] uses a distribution of the form given in eq 1 for a sample with a perfectly aligned director. A similar model in which the concentration of the solution and the flexibility of the wormlike chains is taken into account has been proposed for aramid solutions.[5,6]

In practice, there are three contributions that determine the azimuthal orientation: first, the molecular order with respect to the local director; second, the degree of macroscopic alignment of the director field itself; and third, due to imperfect lateral order (along the c axis), a meridional streak or layer line that will lead to an additional broadening of the experimentally observed azimuthal orientation. This means that the orientational order that is experimentally determined will be a convolution of these three factors. The order parameter that is measured from the azimuthal scans will be written as S_{exp}.

The value of S_{exp} can be determined from the value of the fwhm, assuming that eq 1 is a reasonable approximation for the experimental orientational distribution. For the intensity of the scattered radiation as a function of the angle β we write

$$I(\beta) = I_{\parallel}\exp[\alpha(P_2(\cos(\beta)) - 1)] \quad (2)$$

analogous to eq 1. For $\beta = 0$ or π we obtain the maximum intensity $I_{\parallel}$, and for $\beta = \pm\pi/2$ we find the intensity perpendicular to the direction of the orientation:

$$I_{\perp} = I_{\parallel}\exp(-3\alpha/2) \quad (3)$$

For the angle β_{HM} we find the intensity I_{HM}, halfway between $I_{\parallel}$ and $I_{\perp}$:

$$I_{HM} = (I_{\parallel} + I_{\perp})/2 = I_{\parallel}\exp[\alpha(P_2(\cos(\beta_{HM})) - 1)] \quad (4)$$

This leads to the following equation for α:

$$(1 + \exp(-3\alpha/2))/2 = \exp[\alpha(P_2(\cos(\beta_{HM})) - 1)] \quad (5)$$

This can be solved for α by simple numerical methods, e.g., Newton–Raphson iteration. Using α, we can now calculate the experimental order parameter S_{exp}:

$$S_{exp} = \frac{\int_{-1}^{1} d(\cos(\beta))\exp[\alpha(P_2(\cos(\beta)))P_2(\cos(\beta))]}{\int_{-1}^{1} d(\cos(\beta))\exp[\alpha(P_2(\cos(\beta)))]} \quad (6)$$

The integrals are solved by numerical integration. Using eqs 5 and 6, we can calculate S_{exp} from the fwhm. Calculation of the S_{exp} value directly from the densitograms does not improve the accuracy of the results due to the noise on the signal. Also, a slight error in the background intensity will strongly influence the calculated S_{exp} value. During an experiment S_{exp} will in general depend not only on the shear rate but also on the applied shear strain; in the following we will use $S_{exp}(\infty)$ to denote the steady-state value (for large applied strains).

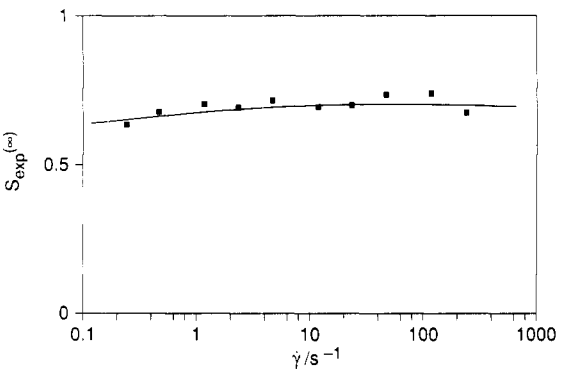

Figure 6. Steady-state orientational order $S_{exp}(\infty)$ as a function of the shear rate.

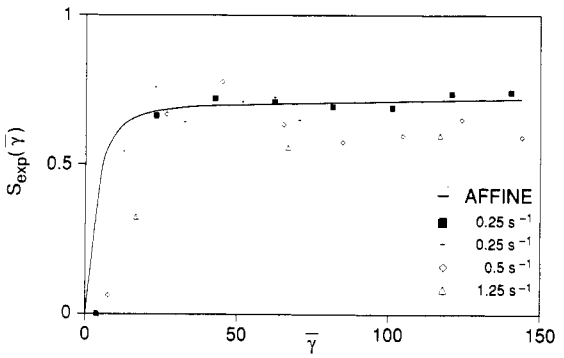

Figure 7. Average orientational order $S_{exp}(\bar{\gamma})$ during start-up experiments as a function of the applied strain for various shear rates as indicated. The drawn curve is from the affine deformation model described in the Appendix.

(iii) Start-up Experiments. In Figure 6 we show $S_{exp}(\infty)$ as a function of the applied shear rate. We observe that the average orientation does not seem to be influenced strongly by the shear rate ($\dot{\gamma}$).

To study the effect of strain we show the results of start-up experiments in Figure 7. The scatter in the results indicates that the reproducibility is not satisfactory; this will be studied in more detail in future experiments.

Here for various shear rates we have determined S_{exp} as a function of the average strain ($\bar{\gamma}$) during the exposure of the film. Using a carousel, it was possible to change films in 10 s, so that together with the required exposure time (30 s), it was possible to do a measurement every 40 s. This limits the number of points that can be measured as the strain is at most 150 strain units and the minimum shear rate was 0.25 s^{-1}. From the results in Figure 7 it is found that the sample, initially with random orientation, is aligned after ca. 20 strain units. Although there might be some effect of the shear rate, the orientation process seems to be essentially determined by the applied strain. Of course, any details in the variation of the order parameter as a function of strain are averaged out by the exposure time of the film.

To try to understand the observed strain dependence of the orientation process, we have calculated an affine deformation model for a simple shear deformation process.

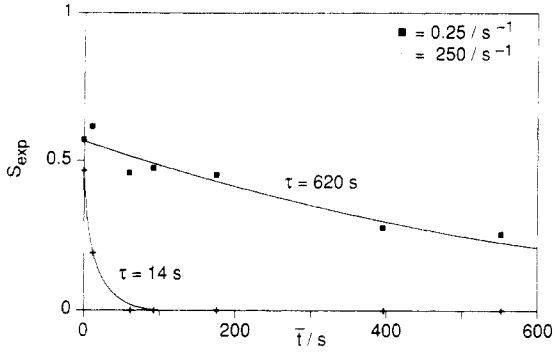

Figure 8. Orientation relaxation curves; the relaxation times τ were calculated by using eq 8.

This model is described in the Appendix. The result for a shear rate of 0.25 s^{-1} (i.e., averaged very 7.5 strain units) is shown in Figure 7. The director order parameter $\bar{P}_2$ from the affine deformation model is scaled to obtain agreement with the experimental results for the large-strain region. The model is only intended to describe the development of the orientational order as a function of strain. By comparing the affine deformation model with the experimental results for 0.25 s^{-1}, we observe that the affine deformation model describes the alignment of the director as a function of strain reasonably well.

(iv) Relaxation Experiments. We have also performed orientation relaxation measurements. The sample was sheared, applying sufficient strain to reach the steady-state orientation, and then the decay of the orientational order was studied as a function of time. The results are shown in Figure 8 for two values of the initial shear rate. It is clear that the decay of the orientational order is much faster for the high initial shear rate of 250 s^{-1} than with the low shear rate of 0.25 s^{-1}. The values for the relaxation times are respectively 14 and 620 s. To calculate the relaxation times, we assumed an exponential decay of the orientational order after shear:

$$S_{exp}(t) = S_{exp}(\infty)e^{-t/\tau} \quad (7)$$

where $S_{exp}(\infty)$ is the steady-state value for the average orientational order and τ is the relaxation time. Due to the required exposure time δt we are measuring an average value that is given by the following equation:

$$[S_{exp}(t)]_{av} = S_{exp}(t)\frac{2\tau}{\delta t}\sinh\left(\frac{\delta t}{2\tau}\right) \quad (8)$$

Here, t is the average time elapsed since the cessation of flow, and δt is the exposure time of the film (i.e., 30 s). If eq 8 is not used, relaxation times on the order of or less than the exposure time will be overestimated. For the two values shown in Figure 8, only the result for 250-s^{-1} pre shear rate is influenced by this effect.

In Figure 9 the relaxation time τ is shown as a function of pre shear rate. In future experiments we will investigate this in more detail for other pre shear rates.

It is possible to obtain "structure relaxation times" from intermittent shear measurements,[1] where the recovery of the transients in the shear stress is studied as a function of the time since the application of the first strain. The results for the structure relaxation from intermittent shear experiments are also shown in Figure 9. We observe that the results for τ from X-ray scattering and from intermittent shear measurements are of the same order of magnitude and show the same general trend. This will be part of a following publication on the rheology and structure of aramid solutions.

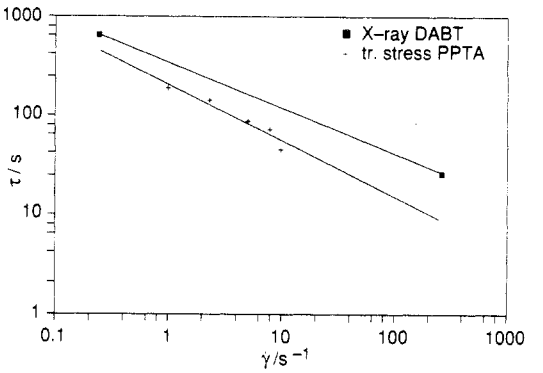

Figure 9. Structure relaxation times from X-ray scattering on a DABT 19.8% (w/w) solution at 20 °C and from intermittent shear experiments on a PPTA 19.8% (w/w) solution at 80 °C.

(v) Coagulation Experiments. In addition to the shear flow experiments, we performed coagulation experiments. Again, we used mica foil as a substrate to allow the radiation to pass through the solution. The solution was aligned by spreading the solution onto a mica foil. The thin layer of solution coagulated due to the presence of water vapor in the air. The coagulation process took several minutes to complete, so that several films could be exposed during the coagulation.

From the films it is seen that the solution coagulates quite suddenly after ca. 150 s. On one film both the diffraction pattern of an uncoagulated solution and that of a coagulated solution can be seen. Two interesting effects are observed: first, extremely sharp equatorial reflections are found in the coagulated sample (this indicates the formation of large crystallites) and second, it is observed that the d value for the 003 reflection increases by ca. 3% and the fwhm value decreases.

We have as yet not succeeded in indexing all the sharp reflections in the coagulated phase. The observed reflections do not correspond to the reflections of the pure DABT polymer; possibly we are dealing with a complicated crystal–solvate phase with H_2SO_4 and water.

As regards the increase of the d value of the 003 reflection, this can possibly be explained by the occurrence of chain stretching during the coagulation. If we use a simple wormlike model for an isolated aramid chain with a persistence length of ca. 29 nm,[7] we can calculate $\langle\cos(\beta)\rangle$ as a function of the distance l between two points along the contour of the chain:

$$\langle\cos(\beta)\rangle = \exp(-l/L_p) \quad (9)$$

The angle β is the angle between the tangent vectors at the points, and L_p is the persistence length. Using for l the d value that is measured for the 003 reflection, we find $\langle\cos(\beta)\rangle = 0.978$. This means that we expect this d value to be ca. 2.2% less than for a stretched chain. This is in reasonable agreement with the observed change in the d value.

Examining the meridional reflections listed in Table I, we also observe that the higher order reflections correspond to larger c-axis values. This is also in qualitative agreement with a wormlike model for the polymer chain, i.e., with eq 9. A quantitative test of this rather simple model would require a higher accuracy for the d values; nevertheless, the observed trends are quite promising.

To obtain the exact change in the d value due to chain flexibility would require a more complicated calculation based on Monte Carlo or molecular dynamics techniques where the average d value is calculated from an ensemble of likely conformers.

Discussion

Although the reproducibility of the average orientational order parameter as determined from X-ray scattering is not all that impressive, we are convinced that the general trends as shown in this paper are correct. The results presented here are similar to results obtained by Odell et al. on PBT (poly(*p*-bis(oxythiazole))) solutions.[8] Our results indicate that the steady-state orientation during shear flow of an aramid solution is more or less independent of the applied shear rate. The influence of the applied strain on the average orientation suggests an affine deformation model to describe the orientation process. Indeed, the simple model given in the Appendix already gives a quite good description of the orientation process.

From earlier observations of the optical textures using polarization microscopy and from depolarization ratio measurements,[1] we concluded that the alignment of the director seems to improve with increasing shear rate. The present X-ray measurements provide compelling evidence that the steady-state orientational order hardly depends on the shear rate (see Figure 4). A possible explanation for these at first contradictory results of optical and X-ray measurements is to assume that although there are many defects (disclinations) in the director field, their contribution to the volume-averaged orientational order (the quantity measured by X-ray diffraction) is small. The optical texture, on the other hand, mainly tells us something about the "disclination dynamics". This implies that contrary to X-ray scattering results, the optical texture is hardly related to the average degree of molecular alignment. This important point will be discussed in more detail in a future publication.

Another point of interest is the interpretation of the rather low values of S_{exp} that are found. We believe that the low value of S_{exp} is caused by broadening of the meridional reflections due to the lateral disorder along the *c* axis. The idea is that if we have a certain degree of lateral order of the chains along their axis, this will also influence the azimuthal width of the meridional reflections. Depending on the degree of lateral order, we will either observe a 00*l* plane (a streak) or a 00*l* point in reciprocal space for a perfectly oriented "domain". For a crystalline domain we expect a point, and for a perfectly oriented domain with no lateral correlation we expect a streak for the meridional reflections. In practice, a certain degree of lateral order (along the molecular *c* axis) is expected, which will lead to an apparent broadening of the meridional reflections. This broadening effect can possibly be estimated by comparing the fwhm values for various orders of the 00*l* reflections. The lower order reflections are predicted to be less sensitive to this axial shift factor.[9] At the moment such a comparison cannot be done, as the measurement of higher order reflections would require longer exposure times than were used in the experiments described here.

Another approach is to decompose the measured S_{exp} value into various components. It will approximately hold that

$$S_{exp} = K\bar{P}_2\langle P_2\rangle \tag{10}$$

where $\langle P_2\rangle$ is the molecular order parameter, $\bar{P}_2$ is the director order parameter, and K is an unknown constant due to the lateral disorder. Equation 10 is based on the closure relation for generalized spherical harmonics or Wigner matrices.[10] Assuming a uniaxial orientation on a local and on a macroscopic scale, the convolution of orientational distributions reduces to taking the product of the Legendre series coefficients. This is analogous to the more familiar rule for Fourier series.

Using eq 10, we can now divide out the contribution $K\langle P_2\rangle$ as the local structure is expected to be more or less independent of the application of an external flow field. This is a reasonable approximation for the present case where the local molecular order parameter $\langle P_2\rangle$ is quite high, say 0.93 or more.[5,6] After S_{exp} is divided by $K\langle P_2\rangle$, the director order parameter is found which can be compared, e.g., to the affine deformation model from the Appendix. In principle, a better value for the orientational order might be obtained by using the azimuthal orientation of the equatorial reflections. However, the equatorial reflections are much weaker than the meridional reflections, so that this is not very suitable for measurements as a function of strain, due to the much longer exposure times that would be required.

Acknowledgment. We thank Prof. H. N. W. Lekkerkerker for stimulating discussions and his continued interest in this work. In addition, thank the personnel at Daresbury synchrotron laboratory for their help with the experiments and especially Mr. Phil Hayward for this assistance in getting the equipment there on time. Also, we thank the mechanical engineering workshops at Akzo Research Laboratories Arnhem for assistance in modifying the microshear apparatus. Finally, we thank ing. Schaap of the fiber physics department (Akzo Fibres and Polymers Division) for letting us use the image analysis equipment for measuring the azimuthal half-width and Dr. van Blokland of the technical physics department for the X-ray contour plot.

Appendix

To calculate the orientation due to a simple shear deformation we used the following affine deformation model. It should be noted that an affine deformation model gives the highest possible degree of orientation due to the absence of any slip. A simple shear deformation is conveniently described by the deformation tensor $\mathbf{F}_j^i$, where

$$x_j' = \mathbf{F}_j^i x_i$$

On an orthonormal coordinate system it holds that

$$\mathbf{F}_j^i = \begin{bmatrix} 1 & 0 & 0 \\ 0 & 1 & 0 \\ \gamma & 0 & 1 \end{bmatrix}$$

The orientational distribution is calculated as a function of the shear strain γ using a statistical method. Unlike an elongational deformation, where the symmetry axis is well defined and simple analysis can be used, the analytical calculation of the orientational distribution function and order parameters for a simple shear deformation appears to be rather complicated.

The statistical method is as follows: (i) generate a random unit vector from an isotropic orientational distribution (φ from $[0,2\pi]$ and cos (θ) from $[1,-1]$); (ii) transform this vector using $\mathbf{F}_j^i(\gamma)$; (iii) calculate the polar angles φ' and θ' and appropriate order parameters such as $P_2(\cos(\theta')) = (3\cos^2(\theta') - 1)/2$ and $D = \sin^2(\theta')\cos(2\varphi')$; (iv) $N = N + 1$; (v) if $N < N_{max}$ goto *i*.

From the set of values of P_2 and D averages can be calculated for each shear strain γ. In Figure 10 the results are shown for $\bar{P}_2$, the orientational order parameter, and $\bar{D}$, the biaxiality parameter. These order parameters can be calculated by using the following analytic

approximations:

$$\bar{P}_2(\gamma) = \left[1 - \frac{3\gamma}{2\gamma^2 + 90}\right]\left[\frac{\gamma^2}{\gamma^2 + 6}\right]$$

$$\bar{D}(\gamma) = \frac{\gamma(1 - \exp(-3/2\gamma))}{\gamma + 10(1 - \exp(-3/2\gamma))}$$

The accuracy of these approximations over the whole strain range can be seen in Figure 10. The analytic approximations were obtained by first analyzing the asymptotic behavior of the statistical results for small and large strains. Then an equation interpolating between these asymptotic regions was obtained by a trial-and-error method. The asymptotic behavior is given by

small γ

$$\bar{P}_2(\gamma) = \gamma^2/6$$

$$\bar{D}(\gamma) = \gamma/10$$

large γ

$$\bar{P}_2(\gamma) = 1 - 3/(2\gamma)$$

$$\bar{D}(\gamma) = 3/(2\gamma)$$

In Figure 10 we also show the result for an elongational deformation as a function of γ ($a = 1 + \gamma$, $x' = x/a^{1/2}$, $y' = y/a^{1/2}$, $z' = za$). This is given by the Kuhn–Grün equation:[11]

$$\bar{P}_2(a) = \frac{2a^3 + 1}{2(a^3 - 1)} - \frac{3a^3}{2(a^3 - 1)^{3/2}} \arctan\left(\sqrt{(a^3 - 1)}\right)$$

Of course, for an elongation deformation $\bar{D} = 0$ from symmetry arguments. It is observed that an elongational deformation provides a much more efficient orientation than a simple shear deformation. In the symptotic region for large γ the Kuhn–Grün equation can be approximated by

$$\bar{P}_2(\gamma) = 1 - 3\pi/(4\gamma^{3/2})$$

This stronger γ dependence for an elongation deformation explains the rather poor reputation of shear deformation for the formation of high-modulus materials. One conclusion of these calculations is that if sufficient strain can be applied, the degree of orientation due to simple shear can be just as high as that obtained from elongation, although in practice applying a shear strain of ca. 40 is often not possible.

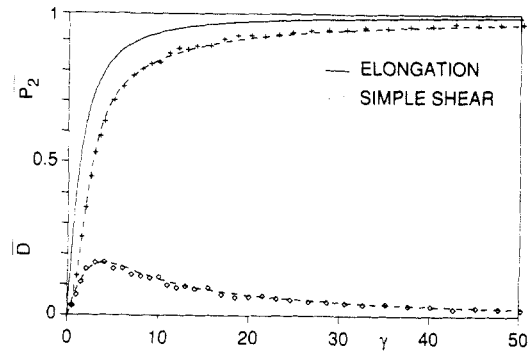

Figure 10. Orientational order parameters $\bar{P}_2$ (+) and $\bar{D}$ (◇) as a function of shear strain γ from the affine deformation model using 2000 ($=N_{max}$) iterations per strain value. The analytic approximations for $\bar{P}_2$ and $\bar{D}$ given in the text are shown by the dashed curves. The result for an affine elongation is also shown (only $\bar{P}_2$) for comparison as a function of γ, where $a = 1 + \gamma$ in the Kuhn–Grün equation.

References and Notes

(1) Doppert, H. L.; Picken, S. J. *Mol. Cryst. Liq. Cryst.* **1987**, *153*, 109.
(2) Blok, P.; Picken, S. J.; Verwaaien, H. H. T. *De Constructeur* **1987**, *26* (12), 44 (in Dutch).
(3) Mabis, A. J. *Acta Crystallogr.* **1962**, *15*, 1152.
(4) Maier, W.; Saupe, A. *Z. Naturforsch.* **1959**, *14a*, 882; **1960**, *15a*, 187.
(5) Picken, S. J. *Macromolecules* **1989**, *22*, 1766.
(6) Picken, S. J. *Macromolecules* **1990**, *238* 464.
(7) Ying, Q.; Chu, B. *Makromol. Chem., Rapid Commun.* **1984**, *5*, 785.
(8) Odell, J., et al., to be published in *Polym. Commun.*
(9) Vainshtein, B. K. *Diffraction of X-rays by Chain Molecules*; Elsevier: Amsterdam, 1966; Chapter VI, pp 274–281.
(10) Zannoni, C. In *Molecular Physics of Liquid Crystals*; Luckhurst, G. R., Gray, G. W., Eds.; Academic: London, 1979; pp 51–83.
(11) Kuhn, W.; Grün, F. *Kolloid-Z.* **1942**, *101*, 248.